Molecular Therapy
Oncology
Original Article

Electrophilic proximity-inducing synthetic adapters enhance universal T cell function by covalently enforcing immune receptor signaling

Nickolas J. Serniuck,[1,2,4] Eden Kapcan,[1,2,4] Duane Moogk,[1,2,3] Allyson E. Moore,[1,2,3] Benjamin P.M. Lake,[1,2,4] Galina Denisova,[2] Joanne A. Hammill,[1,2,3] Jonathan L. Bramson,[1,2,3] and Anthony F. Rullo[1,2,3,4]

[1]Centre for Discovery in Cancer Research, McMaster University, Hamilton, ON, Canada; [2]McMaster Immunology Research Centre, McMaster University, Hamilton, ON, Canada; [3]Department of Medicine, McMaster University, Hamilton, ON, Canada; [4]Department of Chemistry and Chemical Biology, McMaster University, Hamilton, ON, Canada

Proximity-induction of cell-cell interactions via small molecules represents an emerging field in basic and translational sciences. Covalent anchoring of these small molecules represents a useful chemical strategy to enforce proximity; however, it remains largely unexplored for driving cell-cell interactions. In immunotherapeutic applications, bifunctional small molecules are attractive tools for inducing proximity between immune effector cells like T cells and tumor cells to induce tumoricidal function. We describe a two-component system composed of electrophilic bifunctional small molecules and paired synthetic antigen receptors (SARs) that elicit T cell activation. The molecules, termed covalent immune recruiters (CIRs), were designed to affinity label and covalently engage SARs. We evaluated the utility of CIRs to direct anti-tumor function of human T cells engineered with three biologically distinct classes of SAR. Irrespective of the electrophilic chemistry, tumor-targeting moiety, or SAR design, CIRs outperformed equivalent non-covalent bifunctional adapters, establishing a key role for covalency in maximizing functionality. We determined that covalent linkage enforced early T cell activation events in a manner that was dependent upon each SARs biology and signaling threshold. These results provide a platform to optimize universal SAR-T cell functionality and more broadly reveal new insights into how covalent adapters modulate cell-cell proximity-induction.

INTRODUCTION

Bifunctional proximity-inducing small molecules, aka molecular glues, are being used increasingly in therapeutics modalities. Natural agents like cyclosporin A, rapamycin, and FK506 have inspired synthetic designs, such as PROTACS, Bicycles, and ARMs. We are particulary interested in the use of such bifunctional molecules to bridge components of the immune system with tumor cells to mediate anti-tumor immune function.[1,2]

Engineering immune cells to express synthetic antigen receptors (SARs), such as the well-described chimeric antigen receptor (CARs), has revolutionized cell therapy for cancer and is rapidly being deployed for non-malignant diseases.[3–8] Conventional SARs are introduced into therapeutic T cells via genetic engineering; however, target specificity is typically limited to one, or two, tumor target(s). Given the potential for tumors to escape SAR-engineered T cell (SAR-T cell) treatment by antigen loss, and the heterogeneous nature of many tumor types, multi-targeted engineered T cell products are of significant interest.[9] However, given the vast number of potential targets[10,11] and the high cost of T cell manufacturing, generating multiple separate SAR-T cell batches per patient is an ineffective solution. A flexible platform that minimizes T cell manufacturing while maximizing the spectrum of antigen targets is highly desirable. "Universal" SARs are programmed with target specificity *after* the engineered T cells are manufactured through *molecular adapters* that link the SAR-expressing T cells to the tumor.[12,13] By creating a library of molecular adapters, a T cell engineered with a single universal SAR can be directed against multiple tumor targets and tailored to the antigenic repertoire of the tumor, thereby reducing the need for multiple engineering runs to produce T cells with distinct antigen specificity. Preclinical studies have confirmed the utility of this strategy in the treatment of hematologic and solid tumor models using a variety of donor moieties[14–31] and the approach is currently being tested in clinical trials.

Numerous molecular adapter approaches have been evaluated for templating ternary complexes that bridge universal CARs with tumor antigens.[14–31] Bifunctional small molecule adapters are attractive tools for directing universal CARs due to their ease of production, high tumor penetrance, and low immunogenicity. We

Received 18 April 2024; accepted 21 June 2024;
https://doi.org/10.1016/j.omton.2024.200842.

Correspondence: Jonathan L. Bramson, Office of the Vice Dean Research, Faculty of Health Sciences, McMaster University, HSC 2E17, 1280 Main St West, Hamilton, ON L8S 4K1, Canada.
E-mail: bramsonj@mcmaster.ca
Correspondence: Anthony Rullo, McMaster University, MDCL 4015, 1280 Main St West, Hamilton, ON L8S 4K1, Canada.
E-mail: rulloa@mcmaster.ca

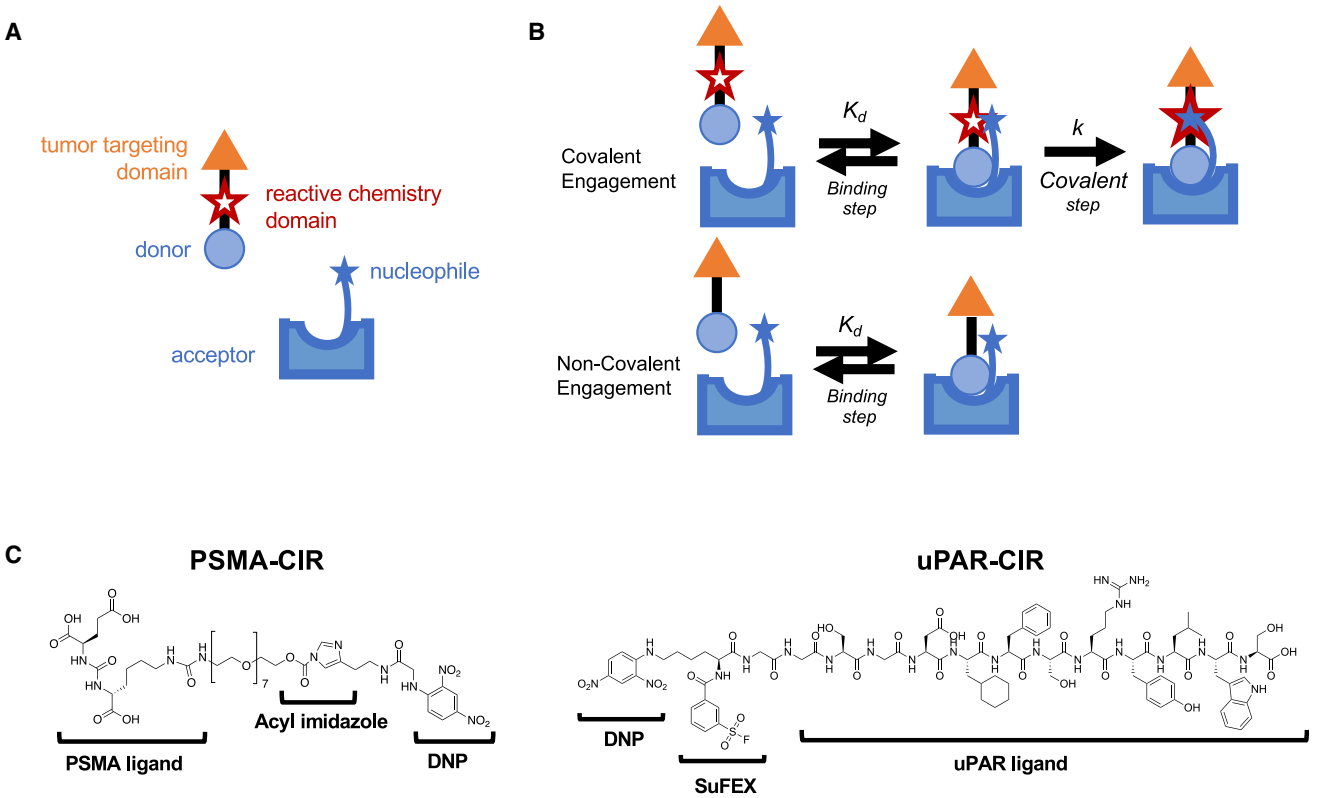

(legend on next page)

reasoned that covalent attachment of the small molecule adapter to a universal receptor could enhance functionality of the receptor. In this article, we describe a universal synthetic receptor system designed to pair with electrophilic bifunctional adapters that bind covalently to the receptor through affinity-induced labeling with no enzymatic requirement. Termed *covalent immune recruiters* (CIRs) (Figure 1A), these adapters are composed of (1) a "donor" domain that binds to an "acceptor" (e.g., scFv), (2) a reactive electrophile domain, and (3) a tumor-targeting domain (Figure 1A). CIRs bind to an acceptor group through their donor domain, resulting in binding-induced covalent labeling via the electrophilic covalent chemistry that reacts with a nucleophilic amino acid within the binding pocket of the acceptor (Figure 1B). The modular design of CIRs offers a great deal of functional flexibility as different chemistries can be used to tune reaction kinetics and adapter stability, while a wide range of ligands can be used to direct CIRs, including small molecules, peptides, etc.

To date, only universal CARs have been described, so it remains unknown whether other classes of SARs would be suitable for combination with molecular adapters. Two other receptors of interest are the T cell antigen coupler (TAC) receptor developed by our group[32] and a KIR2DS2-based receptor that transmits the intracellular signal via association with DAP12 (KIR-CAR).[33] The various SARs manifest some similarities in terms of eliciting T cell cytotoxicity against tumor targets, but they also display distinct biologies with regard to long-term functionality and persistence of the engineered T cells. Whether the different activation requirements of conventional CAR, TAC, and KIR-CAR platforms influence their ability to be "universalized" with molecular adaptors remains to be determined.

Here, we describe CIRs based on two distinct electrophilic chemistries, acylimidazole esters and aryl sulfonyl fluorides (SuFEX), for use with universal SARs based on CAR, KIR-CAR, and TAC scaffolds. We demonstrate that the CIRs can direct engineered T cell function in a highly selective manner. Irrespective of the chemistry, tumor-targeting moiety, or synthetic antigen receptor design, the CIRs outperformed their non-covalent counterparts in all situations. Moreover, through detailed assessment, we determined that *covalent* attachment of the molecular adapters enhanced the functionality of all universal SARs tested when compared with adapters that do not achieve covalent attachment. We expect these results will be relevant to all bifunctional adapter molecules, irrespective of whether they bind synthetic receptors or natural receptors.

RESULTS

CIRs efficiently covalently engage universal SARs

Here, we sought to characterize the utility of CIRs to direct T cells engineered with SARs. The CIR design is shown in Figure 1A, left side. A matched bivalent molecule that lacks the covalent binding group ([N] CIR) is included in all experiments to assess the biological importance of covalency. The amount of (N)CIR bound to a given acceptor is a function of the equilibrium dissociation constant (Figure 1B, lower schematic), whereas covalent attachment of the CIR to the acceptor group leads to a predominance of the "bound" state upon reaction completion, independent of the dissociation constant but influenced by the reaction kinetics (Figure 1B, upper schematic). Using an anti-DNP scFv derived from an antibody that was validated as a CIR acceptor in our previous work,[34] we designed a series of universal SARs using the following scaffolds: second-generation CD28-containing CAR, DAP12-based CAR (KIR-CAR), and TAC receptor (Figure 1D). Primary human $\alpha\beta$-T cells were engineered to express these universal SARs and surface expression was determined through myc-tag detection (present in all SARs). While the DNP-KIR-CAR and DNP-CAR were expressed at similar levels on the engineered T cell, the DNP-TAC was expressed at a lower level (Figures 1E and S1). Despite comparable surface expression, we observed minimal tonic signaling in T cells engineered with the DNP-KIR-CAR, whereas T cells engineered with the DNP-CAR displayed substantial tonic signaling as evidenced by basal tumor necrosis factor (TNF)α and interferon (IFN)γ cytokine production (Figure 1F).

To confirm that CIRs can selectively bind universal SARs, we labeled engineered T cells using a CIR equipped with an acyl imidazole reactive electrophile and desthiobiotin in place of a tumor-targeting ligand (AI-DTB CIR; Figure 2A). CIR labeling of DNP-specific TAC receptor-engineered T cells was measured by flow cytometry. To address the contribution of covalent binding group in the CIR, we included a matched adaptor that lacks the reactive electrophile (DTB-(N)CIR; Figure 2A). T cells were incubated with 1 μM CIR or (N)CIR overnight at 4° to prevent receptor internalization and washed prior to staining to assess binding to the DNP-TAC. Only the combination of AI-DTB CIR and anti-DNP-TAC produced a shift in fluorescence relative to TAC-T cells that were not labeled with CIR (Figures 2B and S2C). We observed no increase in fluorescence when TAC-T cells were incubatated with DTB-(N)CIR. The (N)CIR, which still binds anti-DNP scFv with low nm affinity and nearly saturates all receptors at equilibrium (>95% receptor occupancy), also dissociates on the timescale of the T cell washing steps

Figure 1. Anti-DNP SAR αβ T cell production and CIR interaction

(A) General structure and components of CIR (upper left) and a generic acceptor (lower right). (B) Steady-state interaction between the donor moiety and an acceptor leads to a balance of bound/unbound CIR/(N)CIR. In the case of the CIR, a subsequent covalent labeling step occurs when the covalent reactive chemistry is placed in close proximity to a nucleophilic amino acid. Covalent attachment of the CIR to the acceptor molecule leads to a state where the tumor binding domain is irreversibly bound to the acceptor molecule. (C) Structure of the DNP-acyl imidazole-glutamate-urea-lysine CIR (PSMA-CIR) and the DNP-Sufex-uPAR peptide CIR (uPAR-CIR). (D) An illustration of the receptor design and selection. All receptors employ the same anti-DNP as the acceptor. (E) Expression of the anti-DNP scFv containing TAC, KIR-CAR, and CAR on αβ T cells. Cells were gated on singlets > $CD4^+/CD8^+$ > Myc^+. Both CD4 and CD8 T cell population showed the same results, CD4-positive T cells are shown in this figure (see Figure S1 for gating and repeats). (F) Analyzed intracellular cytokine levels of TNF-α and IFN-γ of each universal SAR-engineered T cell when cultured in media alone to assess tonic signaling of each receptor.

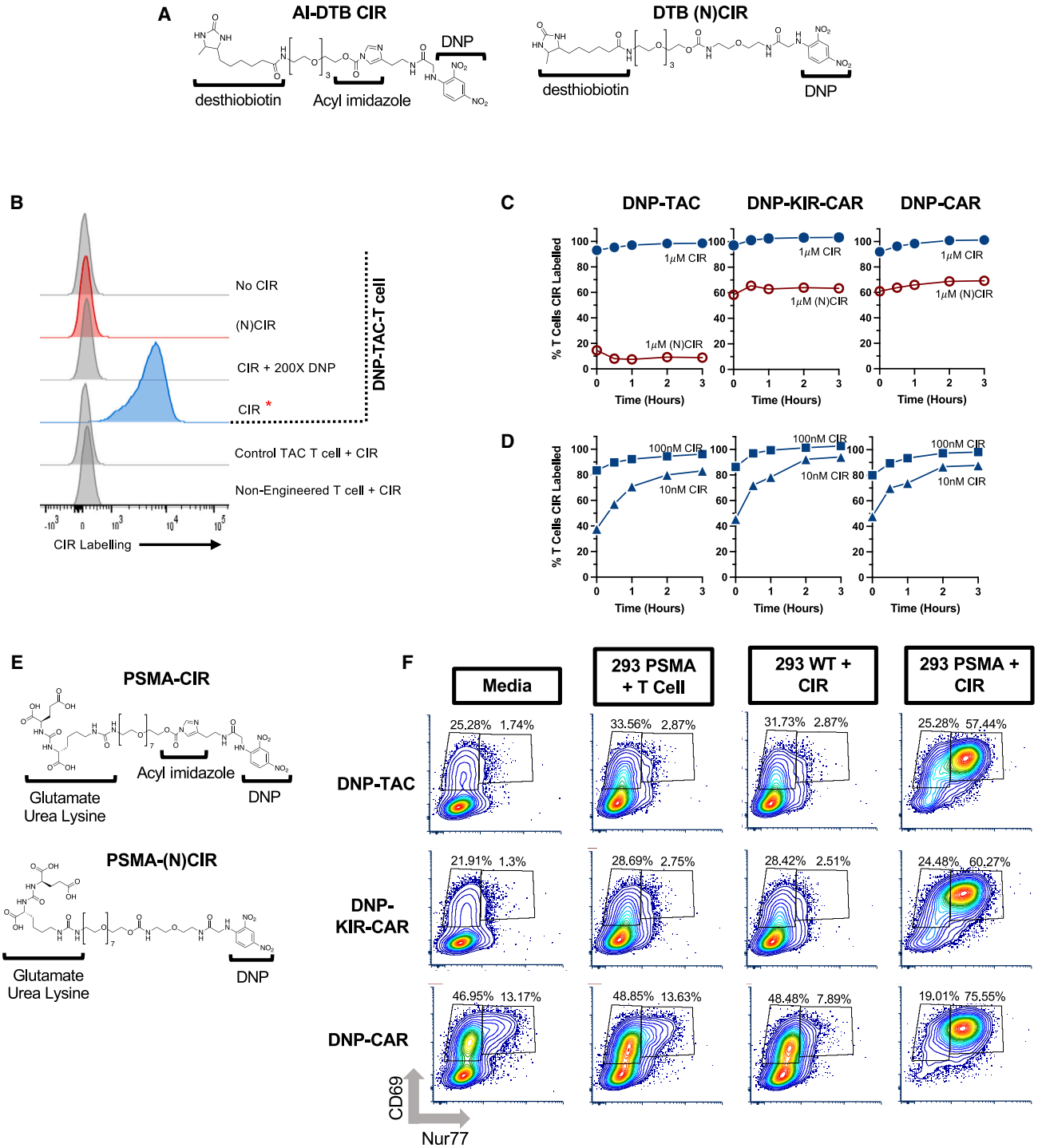

Figure 2. CIRs produce selective antigen-specific activation of universal SARs

(A) Structure of the DNP-acyl imidazole-desthiobiotin (AI-DTB CIR) and DNP-desthiobiotin (DTB (N)CIR). (B) DNP-TAC-T cells were labeled with AI-DTB CIR or AI-DTB CIR followed by streptavidin-PE. Non-anti-DNP scFv-containing cells (Control TAC-T cell) and non-engineered T cells were also labeled with AI-DTB and streptavidin-PE. As negative controls, DNP-TAC T cells were incubated with streptavidin-PE without prior labeling with CIR (No CIR) or the DNP-TAC T cells were labeled with AI-DTB CIR in the presence of 200-fold excess DNP (CIR +200X DNP). Both CD4 and CD8 T cell population showed the same results, CD8 T cell population used for this figure (see Figure S2 for gating and repeats). (C and D) Analysis of AI-DTB CIR rate of labeling over 3 h at a range of concentrations with TAC-, KIR-CAR-, and CAR-engineered T cells. DTB (N)CIR control is also included to show importance of covalent binding. Cells were gated on singlets > $CD4^+/CD8^+$ > streptavidin-PE^+, y axis corresponds to % of T cells labeled with

(legend continued on next page)

in this experiment. These observations support the importance of a covalent linkage to stabilize the attachment of the molecular adapter to the universal TAC. To confirm selectivity, the AI-DTB CIR was incubated with (1) non-engineered T cells and (2) T cells expressing a TAC that does not bind DNP. Neither control T cell bound the CIR (Figure 2B), confirming that CIR selectively engages the anti-DNP-TAC receptor. Finally, the anti-DNP-TAC-T cells did not bind the CIR in the presence of excess competitor DNP (Figure 2B), which supports the selectivity of the CIR for the anti-DNP acceptor. The same results were observed in the context of DNP-CAR and DNP-KIR-CAR constructs (Figure S2B).

Next, using the AI-DTB CIR and DTB-(N)CIR, we measured the rate of adapter loading across a range of concentrations (10 nM–1 μ M; Figures 2C, 2D, and S3B) at room temperature over 3 h. In these experiments, incubations with CIR gave rise to time-dependent increases in cell fluorescence consistent with covalent bond formation, in contrast to control experiments using (N)CIR. We observed both 1 μM and 100 nM CIR labeled the majority of the engineered T cells within a few minutes and >90% of engineered T cells within 3 h, supporting rapid covalent labeling kinetics (Figures 2C, 2D, and S3B). Even at the lowest concentration of CIR (10 nM), 40% of the T cells were labeled within the first few minutes and approximately 80% of the T cells were labeled within 3 h, independent of the universal SAR that was tested (Figures 2D and S3B). As in Figure 2B, the DTB-(N)CIR failed to remain bound to the TAC receptor, whereas DTB-(N)CIR remained bound to the DNP-KIR-CAR and DNP-CAR on some of the engineered T cells (Figures 2C and S3B) at 1 μ M. This binding, however, saturated early and did not increase over time, whereas the AI-DTB CIR demonstrated a time-dependent increase in labeling of both DNP-KIR-CAR and DNP-CAR. Enhanced loading of the universal SARs by CIR relative to (N)CIR was observed across all concentrations (Figure S3C).

CIRs selectively activate universal SARs in a tumor antigen-dependent manner

Upon verification that CIRs can selectively, covalently engage all three universal receptors, we evaluated their ability to activate T cells engineered with the universal SARs. We used a previously validated CIR that employs the acyl imidazole labeling chemistry and glutamate-urea-lysine group to target prostate specific membrane antigen (PSMA) (Figure 2E).[34] A matched (N)CIR that contains the DNP and glutamate-urea-lysine but lacks the reactive chemistry was included to probe the effects of covalent stabilization (Figure 2E). Engineered T cells were co-cultured with PSMA-expressing target cells (293-PSMA) and 100 nM CIR for 4 h and T cell activation was measured based on expression of CD69, a key marker in early T cell lymphocyte activation, and Nur77, a transcription factor taken as a measure of integrated immunoreceptor signaling (Figure 2F).[35] The basal activation state for each engineered T cell product was measured by culturing T cells in media alone and by co-culturing T cells with 293-PSMA cells in the absence of CIR. As a control for off target activation, T cells and CIR were co-cultured with wild-type 293 cells (293-WT) which do not express PSMA. We observed little change in activation markers on T cells cultured in medium, co-cultured with 293-PSMA alone or co-cultured in 293-WT + CIR (Figure 2F). In contrast, when T cells were co-cultured with 293-PSMA in the presence of CIR, we observed robust upregulation of CD69 and Nur77 on all engineered T cell populations (Figure 2F), confirming the antigen-selectivity of the universal SAR/CIR combination. The greatest activation was observed on DNP-CAR-T cells. The difference in activation is likely due to the high basal activation state of the DNP-CAR-T cells (13% of T cells express CD69 and Nur77 in medium alone) compared with DNP-KIR-CAR T cells and DNP-TAC T cells (only 1%–2% of T cells express CD69 and Nur77 in medium alone). High basal activation of the DNP-CAR-T cells is consistent with tonic CAR signaling and the basal production of cytokine observed in Figure 1F.

Covalent engagement of universal SARs enhances engineered T cell function

To determine whether the activation induced by CIR and (N)CIR engagement correlates with functional outcomes, we assessed antigen-dependent cytokine production, cytotoxicity, and proliferation of SAR-engineered T cells. The frequency of SAR-engineered T cells stimulated to produce effector cytokines TNFα and IFNγ was measured following a 4-h co-incubation of the T cells with 293-PSMA cells and a range of CIR/(N)CIR concentrations (1 nM–100 nM) (Figure 3A). Notably, the (N)CIR was unable to elicit cytokine production from TAC-T cells at any concentration, whereas the CIR displayed a dose-dependent capacity to activate cytokine production. With the DNP-KIR-CAR, the 100-nM (N)CIR could enable T cells to produce cytokine; however, 100-nM CIR facilitated a significant increase in cytokine production. At lower concentrations, (N)CIR was markedly less effective than CIR at eliciting a cytokine response from KIR-CAR T cells. In the case of DNP-CAR-T cells, both CIR and (N)CIR elicited comparable cytokine production at 100 nM, but the CIR promoted cytokine production in a significantly higher number of DNP-CAR-T cells at limiting concentrations (1 nM, 10 nM). To control for antigen specificity, SAR-engineered T cells were co-cultured with (1)100 nM CIR in media alone, (2) 100 nM CIR in the presence of 293-WT cells, or (3) 293-PSMA cells without adapter. DNP-TAC- and DNP-KIR-CAR-T cells displayed nominal cytokine production in these control conditions, which reinforces the antigen-specific nature of the CIR/(N)CIR activation. As

CIR or (N)CIR. CD4 and CD8 labeling results were averaged and graphed (see Figure S3 for gating and repeats). (E) Structure of the DNP-acyl-imidazole-glutamate-urea-lysine CIR (PSMA-CIR) and DNP-glutamate-urea-lysine (N)CIR (PSMA-(N)CIR). (F) Anti-DNP SAR-engineered αβ T cells with 100 nM PSMA-CIR, or media alone, were incubated with either wild-type or PSMA-engineered HEK-293 cells and CD69 and Nur77 were measured by flow cytometry. Data were gated on live > singlets > $CD4^+$/$CD8^+$. The fraction of T cells expressing only CD69 or CD69 and Nur77 is shown in each flow plot (see Figure S8 for gating). Both the CD4 and CD8 T cell population revealed the same results. The CD4 T cell population is shown in this figure.

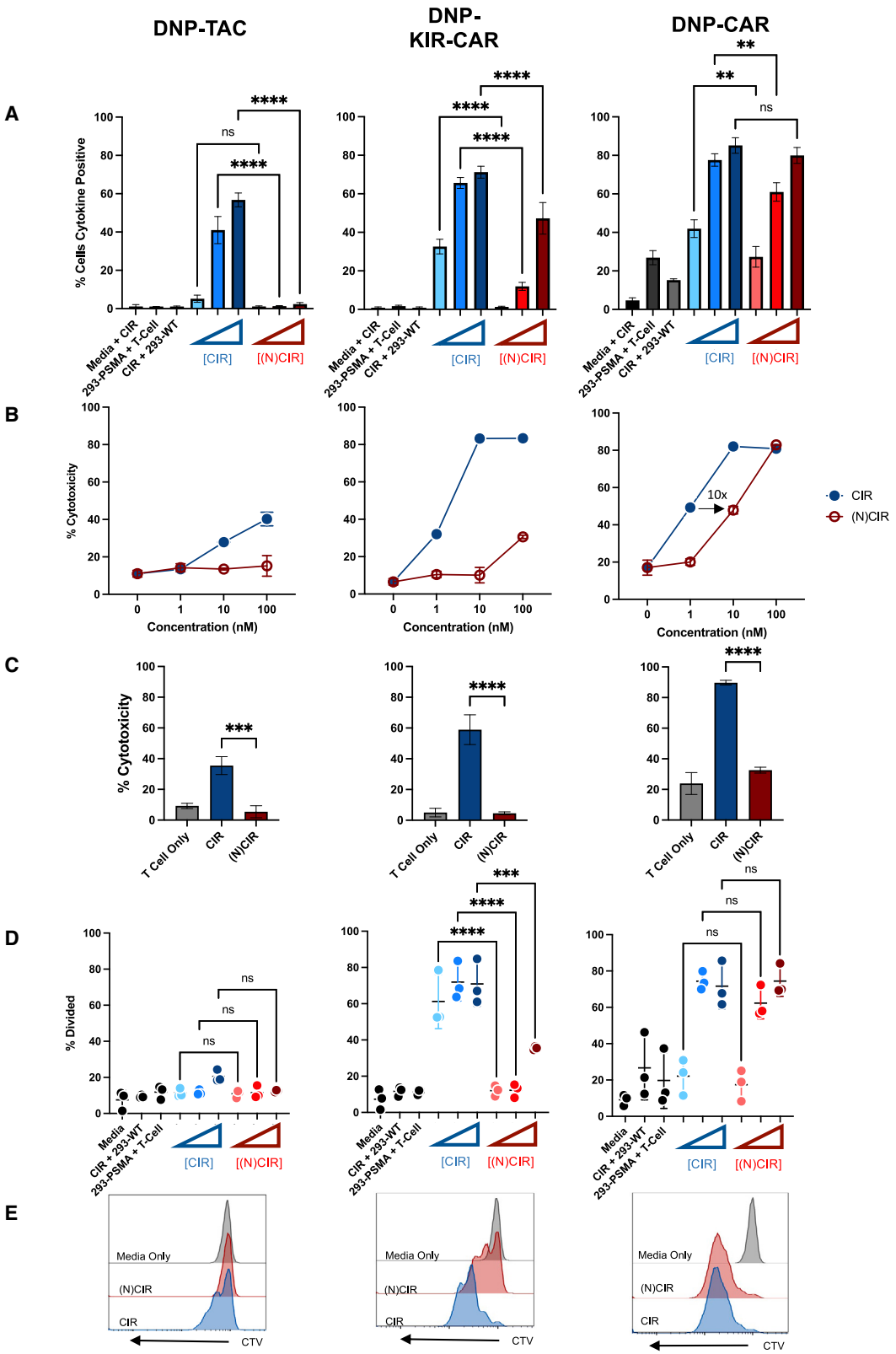

(legend on next page)

observed in Figure 1E, the DNP-CAR-T cells consistently displayed higher levels of cytokine production in all controls.

We next assessed SAR-T cell cytotoxicity against LNCaP prostate cancer cells, which endogenously express PSMA. The SAR-T cells were incubated with LNCaP tumor cells for 3 days in the presence of varying concentrations of CIR or (N)CIR (Figure 3B). Consistent with the previous data, the (N)CIR did not elicit cytotoxic function from DNP-TAC-T cells, while significant tumor killing by DNP-TAC-T cells was observed at 10 nM and 100 nM of CIR. High concentrations of (N)CIR (100 nM) elicited modest cytotoxicity by the DNP-KIR-CAR-T cells, but no cytotoxicity manifested at lower concentrations. In contrast, at concentrations of 100 nM and 10 nM, the CIR elicited maximal cytotoxicity from KIR-CAR T cells and significant cytotoxicity was measured at 1 nM CIR. Consistent with the results of the cytokine production assay (Figure 3A), both CIR and (N)CIR elicited comparable cytotoxicity from the DNP-CAR-T cells at high concentrations, while at lower doses, the CIR triggered greater cytotoxicity from the DNP-CAR-T cells, revealing an approximate 10-fold enhancement in activation potential based on the amount of CIR/(N)CIR required to achieve 50% cytotoxicity. Similar outcomes were observed with SAR-T cells produced from two other donors (Figure S4A), as well as when targeting PC3 prostate cancer cells engineered to express PSMA (Figure S4B).

We hypothesized that covalent functionalization of the SAR would enable loading of SAR-T cells with the molecular adapter prior to co-culture with the tumors. To test this hypothesis, we exposed DNP-TAC-, DNP-KIR-CAR-, and DNP-CAR-engineered T cells to saturating levels of CIR or (N)CIR (1 μM) for 1 h at 37°C. Cells were washed thrice and co-cultured with LNCaP cells to measure cytotoxicity using live cell imaging (Figure 3C). T cells pre-incubated in media alone were used as a control to assess basal cytotoxicity. Only functionalization with the CIR rendered the SAR-T cells capable of killing LNCaP cells. Loading of the SAR-T cells with (N)CIR failed to promote cytotoxicity above baseline (Figure 3C; T cell only).

Finally, we assessed SAR-T cell proliferation by loading the T cells with CellTrace Violet (CTV) and stimulating with 293-PSMA cells in the presence of varying concentrations of CIR or (N)CIR (Figure 3D). In the case of DNP-TAC-T cells, proliferation was only observed in the presence of 100 nM CIR and only 20%–30% of the T cells were stimulated to divide. DNP-KIR-CAR T cells were stimulated to proliferate at all concentrations of CIR; in fact, 60%–80% of the population was stimulated to proliferate at 1 nM CIR. In contrast, the (N)CIR was largely ineffective at promoting a proliferative response from DNP-KIR-CAR-T cells where only the highest concentration of (N)CIR (100 nM) was able to stimulate proliferation in ∼40% of the population. No significant difference in proliferation was observed in the context of CD28-CAR-T cells comparing CIRs with (N)CIRs (Figure 3E). These results highlight an important difference between the DNP-KIR-CAR and the DNP-CAR as both stimulate comparable cytokine production and cytoxcity in the presence of limiting concentration of CIR, but the KIR-CAR is more effective in promoting a proliferative response at limiting CIR concentrations. Collectively, these data support that covalent engagement of SARs via CIRs can enhance the activation and anti-tumor function of universal T cells compared with non-covalent analogs.

Covalency remains critical for activating SAR-engineered T cells with a molecular adapter directed against a distinct uPAR tumor antigen

To probe untility of the SAR-CIR platform across different cancer targets, we designed a novel CIR targeting urokinase type plasminogen activator receptor (uPAR) (Figure 4A), an antigen overexpressed across several solid tumor indications.[36] Here, we employed a peptide targeting ligand for uPAR,[36,37] and a distinct labeling chemistry, sulfonyl fluoride exchange chemistry (SuFEX), which has displayed increased hydrolytic stability.[38,39] The specifity of the SuFEX labeling chemistry for the anti-DNP scFv was confirmed using a biotinylated CIR version similar to that which was used in Figure 2B (SuFEX-DTB, Figure 4A). DNP-TAC-T cells were incubated in the presence of the CIR at 1 μ M overnight at 4°C prior to labeling with a streptavidin-PE conjugate for detection of bound adapter via the biotin handle. The AI-DTB CIR and DTB (N)CIR (Figure 2A) were also included as

Figure 3. Functional testing of CIR programmed T cells

(A) T cells were incubated with PSMA-CIR (1 nM, 10 nM, 100 nM), PSMA-(N)CIR (1 nM, 10 nM, 100 nM) in the presence of 293-PSMA cells and stained intracellularly for both interferon gamma (IFN γ) and TNF alpha (TNF α); increasing CIR/(N)CIR concentration is shown as a blue or red triangle, respectively. As negative controls, T cells were incubated in medium alone (Media), wild-type 293 and 100 nM PSMA-CIR (CIR +293-WT), or PSMA-expressing 293 in the absence of CIR (293-PSMA + T cell). The data were gated on singlets > $CD4^+/CD8^+$ > cells producing either IFN γ or TNF α. Both CD4 and CD8 T cell populations revealed the same results and the data in the figure reflect $CD8^+$ T cells (see Figure S9 for gating). (B) LNCaP tumor cells expressing Nuclight Red were co-cultured with anti-DNP SAR-engineered $\alpha\beta$ T cells (E:T of 8:1) and various concentrations of PSMA-CIR (blue symbols) or PSMA-(N)CIR (red symbols) and tumor growth was monitored using live cell imaging. The area under the curve of the LNCaP tumor growth curves was used to determine % cytotoxicity. (C) Anti-DNP SAR-engineered $\alpha\beta$ T cells were labeled with either 1 μM of CIR (blue bar), (N)CIR (red bar), or media alone (gray bar) for 1 h followed by three washes to remove any unbound molecule. The labeled T cells were co-cultured with LNCaP tumor cells expressing Nuclight Red (E:T of 8:1) for cytotoxicity analysis as in (B). (D) Anti-DNP SAR-engineered $\alpha\beta$ T cells were stained with CellTrace Violet (CTV) and co-cultured with PSMA-CIR (1 nM, 10 nM, 100 nM), PSMA-(N)CIR (1 nM, 10 nM, 100 nM), and 293-PSMA cells; increasing CIR/(N)CIR concentration is shown as a blue or red triangle, respectively. As negative controls, T cells were incubated in medium alone (Media), wild-type 293 and 100 nM PSMA-CIR (CIR +293-WT), or PSMA-expressing 293 in the absence of CIR (293-PSMA + T cell). Flow cytometry data were gated on live > singlets > $CD3^+$ > $CD4^+/CD8^+$. FCS Express analysis software was used to determine the proliferation statistics (see Figure S10 for gating). The % of CD8+ T cells that divided over the course of the experiment is shown. The results for $CD4^+$ T cells were similar but not shown. (E) CTV histograms for 100 nM conditions in (D). Statistical analysis for (A) and (C) was performed using ordinary one-way ANOVA, while (D) was performed with a two-way ANOVA, all with correction for multiple comparison (Tukey test) (*$p \leq 0.05$, **$p \leq 0.01$, ***$p \leq 0.001$, ****$p \leq 0.0001$, ns = not significant).

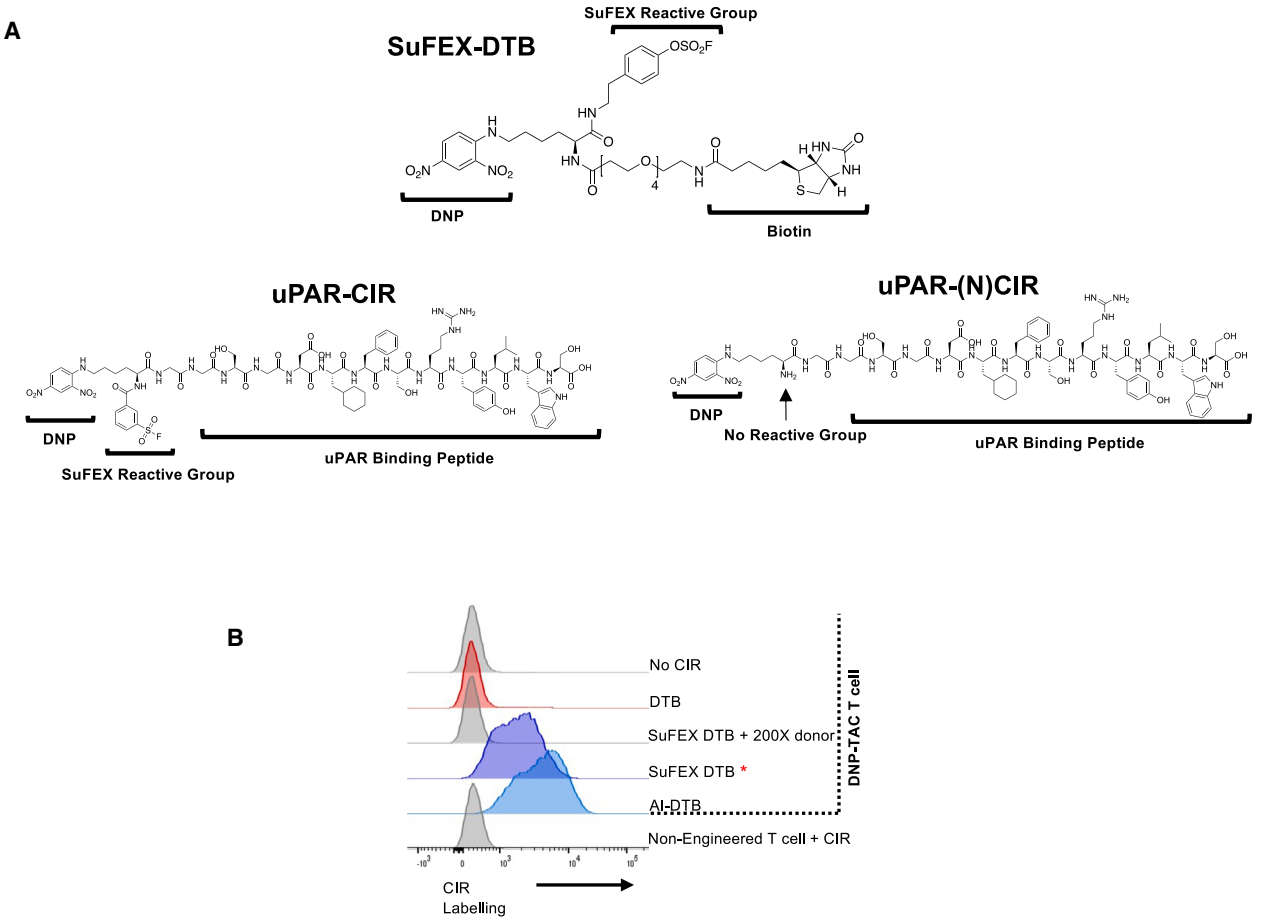

(legend on next page)

positive and negative controls, respectively. In these studies, both CIR probes (SuFEX-DTB and AI-DTB) resulted in positive signal (Figure 4B). We observed no change in MFI relative to control (no CIR) when cells were incubated with the (N)CIR, or when CIR was incubated with non-engineered T cells lacking a DNP SAR. Consistent with selective covalent engagement, no MFI shift was observed when the SuFEX CIR was incubated in the presence of excess DNP competitor.

To determine whether the SuFEX-based covalent molecular adapter can functionalize universal SAR-T cells to target uPAR-expressing tumor cells, we co-cultured anti-DNP SAR T cells with uPAR-expressing A172 glioblastoma tumor cells in medium alone or medium containing 100 nM CIR/(N)CIR. After a 4-h co-incubation, TNFα- and IFNγ-producing cells were enumerated by flow cytometry (Figure 4C). We observed that only the CIR could elicit cytokine production by the SAR-T cells, regardless of the SAR that was used, whereas (N)CIR failed to produce cytokine production above the negative controls (medium, tumor cell only) (Figure 4C). Universal T cells functionalized with CIR were also tested against CRISPR-generated A172 uPAR knockout cells and failed to produce cytokines, supporting the targeting selectivity of adapter-mediated uPAR-targeting universal T cells (Figure S5).

Next, we investigated the cytotoxic potential of DNP SAR T cells programmed with the SuFEX-based CIR. DNP SAR T cells were co-cultured with A172-GFP cells in the presence of varying concentrations of the uPAR-targeting CIR or (N)CIR (Figure 4D). Unlike the results with PSMA-directed molecular adapters, cytotoxicity was only observed with all receptors in the context of the CIR. Similar to the results with the PSMA-directed molecular adapter, only modest cytotoxicity was observed with DNP-TAC-T cells. In contrast, both DNP-KIR-CAR-T cells and DNP-CAR-T cells programmed with CIR demonstrated robust cytotoxicity at 10 nM and 100 nM CIR (Figure 4D). These finding were consistent when SAR-T cell products were generated from two additional, biologically distinct, PBMC donors (Figure S6). These results, in an entirely different setting, reaffirm the functional enhancement that accompanies covalent stabilization of molecular adapter/SAR engagement. Furthermore, we demonstrate that, in some cases, universal SAR function is entirely dependent on covalent attachment of the molecular adapter.

Mechanistic investigations into the origins of covalent functional enhancement

We hypothesized that the functional difference between the CIR and (N)CIR adapters studied in this work could be due to one or a combination of the following: (1) a difference in the frequency of T cell to tumor cell conjugation events or (2) enhanced SAR signaling due to receptor residence time increases that accompany covalent receptor engagement. To test the first hypothesis, we employed confocal microscopy to compare the number of T cell:tumor cell conjugates in the presence of CIR and (N)CIR. DNP-TAC-, DNP-KIR-CAR-, and DNP-CAR-T cells were preloaded with either PSMA-CIR or PSMA-(N)CIR (100 nM or 10 nM) and co-cultured with K562 tumor cells engineered with a PSMA-mCherry fusion protein. Confocal images were used to enumerate the number of T cells (Figure 5A) and T cell:tumor cell conjugates (Figure 5B). In general, we observed comparable degrees in conjugate formation in the presence of either CIR or (N)CIR (Figure 5B) although more conjugates were observed with the DNP-TAC T cells at limiting concentrations (Figure S7).

To address the second hypothesis, we assessed the impact of covalent binding on the formation of an immunological synapse. Here we quantified CD45 phosphatase exclusion at the point of contact between the T cell and the tumor cell.[40] In parallel, we quantified tyrosine phosphorylation (*p*-Tyr) at the synapse as a measure of cellular activation (for example see images in Figure 5C). There was no significant difference in CD45 exclusion between cells conjugated in the presence of CIR or (N)CIR (Figure 5D). Despite comparable synapse formation, conjugates formed in the presence of CIR exhibited a higher *p*-Tyr signal than those formed in the presence of (N)CIR. This suggests that covalent attachment of the molecular adapter drives a stronger activating signal (Figure 5E). Notably, this enhanced *p*-Tyr was only observed in the context of the DNP-KIR-CAR- and DNP-CAR-engineered T cells.

To further investigate the influence of covalent ligation of the molecular adapter on early activation events, we measured phosphorylation of ERK, a kinase immediately downstream of ITAM-based signaling receptors, including SARs (Figure 6A), at early time points following the co-culture of SAR-T cells and 293-PSMA cells in the presence of either CIR or (N)CIR. T cells were pre-incubated with the molecular adapter for 1 h and then co-cultured with 293-PSMA tumor cells in the presence of CIR or (N)CIR. At various time points (see Figure S12

Figure 4. Testing SuFEX CIR labeling and targeting of uPAR

(A) Structures of the DNP-SuFEX-Desthiobiotin (SuFEX-DTB CIR), DNP-Sufex-uPAR peptide CIR (uPAR-CIR), and DNP-uPAR peptide NCIR (uPAR-(N)CIR). (B) DNP-TAC-T cells were labeled with SuFEX-DTB CIR or AI-DTB CIR followed by streptavidin-PE. Non-engineered T cells were also labeled with SuFEX-DTB and streptavidin-PE. As negative controls, DNP-TAC T cells were incubated with streptavidin-PE without prior labeling with CIR (No CIR) or the DNP-TAC T cells were labeled with SuFEX-DTB CIR in the presence of 200-fold excess DNP (CIR +200X DNP). Both CD4 and CD8 T cell populations showed the same results, CD4 T cell population used for this figure. See Figure S2 for gating strategy. (C) SAR-engineered T cells were incubated with uPAR-CIR (100 nM; blue bars), uPAR-(N)CIR (100 nM; red bars) in the presence of A172 cells and stained intracellularly for both interferon gamma (IFN γ) and TNF alpha (TNF α). As negative controls, T cells were incubated in medium and uPAR-CIR without A172 cells (Media+CIR; dark gray bars) or A172 cells without uPAR-CIR (A172 control; light gray bars). The data were gated on singlets > $CD4^+/CD8^+$ > cells producing either IFN γ or TNF α. Both CD4 and CD8 T cell populations revealed the same results and the data in the figure reflect $CD8^+$ T cells (see Figure S9 for gating). (D) A172 cells expressing eGFP were co-cultured with anti-DNP SAR engineered $\alpha\beta$ T cells (E:T of 8:1) and various concentrations of uPAR-CIR (blue circles) and uPAR-(N)CIR (red circles) and tumor growth was monitored by live cell imaging. The area under the curve of the A172 growth curves was used to determine % cytotoxicity. Statistical analysis for (C) was performed using ordinary one-way ANOVA with correction for multiple comparison (Tukey test) (*$p \leq 0.05$, **$p \leq 0.01$, ***$p \leq 0.001$, ****$p \leq 0.0001$, ns = not significant).

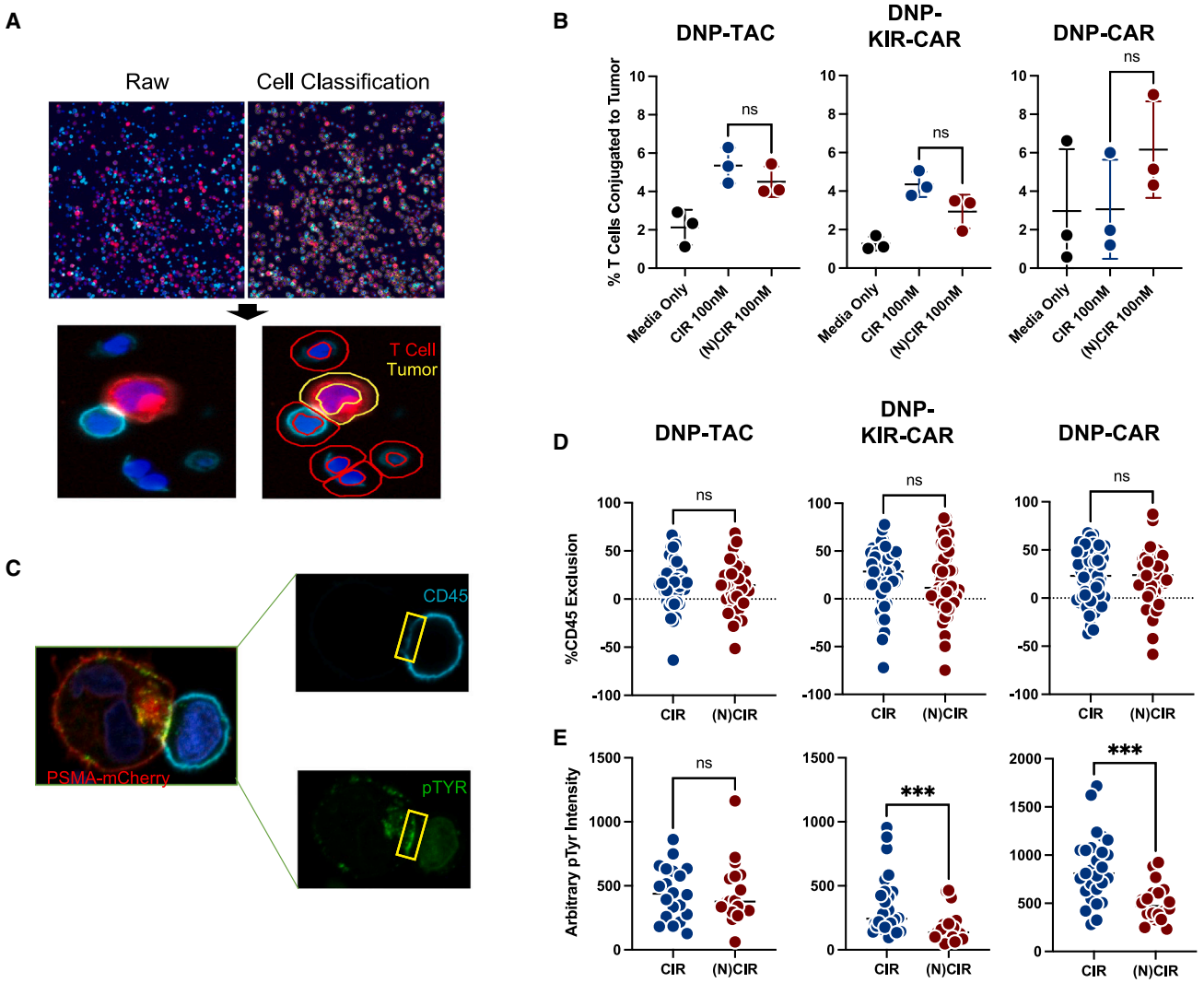

Figure 5. Mechanistic studies of adapter-mediated targeting

(A) Example of a portion of a tiled 20× confocal microscopy image used to identify T cell:tumor cell conjugates. Anti-DNP SAR-engineered αβ T cells were co-incubated with K562 tumor cells engineered to express a PSMA-mCherry fusion protein (red cells). The cells were co-cultured for 30 min, fixed, and stained for CD45 on the T cells (cyan), and nuclear DNA (blue). Qupath software was used to classify and count the number of T cells per image. (B) T cell-tumor cell conjugates were identified manually and combined with the total T cell counts to determine the % of conjugated T cells. (C) Example of a 60× confocal microscopy image used to quantify CD45 phosphatase exclusion and tyrosine phosphorylation at the interface of T cell-tumor cell conjugates. As in (A) and (B), SAR-T cells were co-cultured with 100 nM CIR and NCIR with K562 PSMA-mCherry tumor cells, fixed, and stained for CD45 (cyan), phosphorylated tyrosine (green), and the nuclear DNA (blue). Channels were analyzed individually to assess CD45 exclusion from the synapse (D) and the intensity of tyrosine phosphorylation (E). Statistical analysis for (B) was performed using two-way ANOVA with correction for multiple comparison (Tukey test). Statistical analysis for (D) and (E) was performed using a non-parametric t test (Mann-Whitney test) (*$p \leq 0.05$, **$p \leq 0.01$, ***$p \leq 0.001$, ****$p \leq 0.0001$, ns = not significant).

for gating strategy and validation), cells were collected and the frequency of T cells with phosphorylated ERK expression was determined using flow cytometry (Figure 6B). Across all receptors and adapter concentrations, the CIR induced ERK phosphorylation in a higher fraction of cells than the (N)CIR. The ERK phosphorylation data strongly parallel the results observed with the functional assays in Figures 3 and 4. The data furthers the observations that only the CIR elicited a response from DNP-TAC-T cells, both CIR and (N)CIR could elicit a response from DNP-KIR-CAR-T cells with the CIR eliciting a much stronger response. The DNP-CAR-T cells were activated with both CIR and (N)CIR at more similar frequencies, although the CIR reproducibly prompted ERK phosphorylation in a higher fraction of T cells.

To investigate events farther downstream, we compared Nur77 and CD69 upregulation (Figure 6A) following co-culture of SAR-T cells

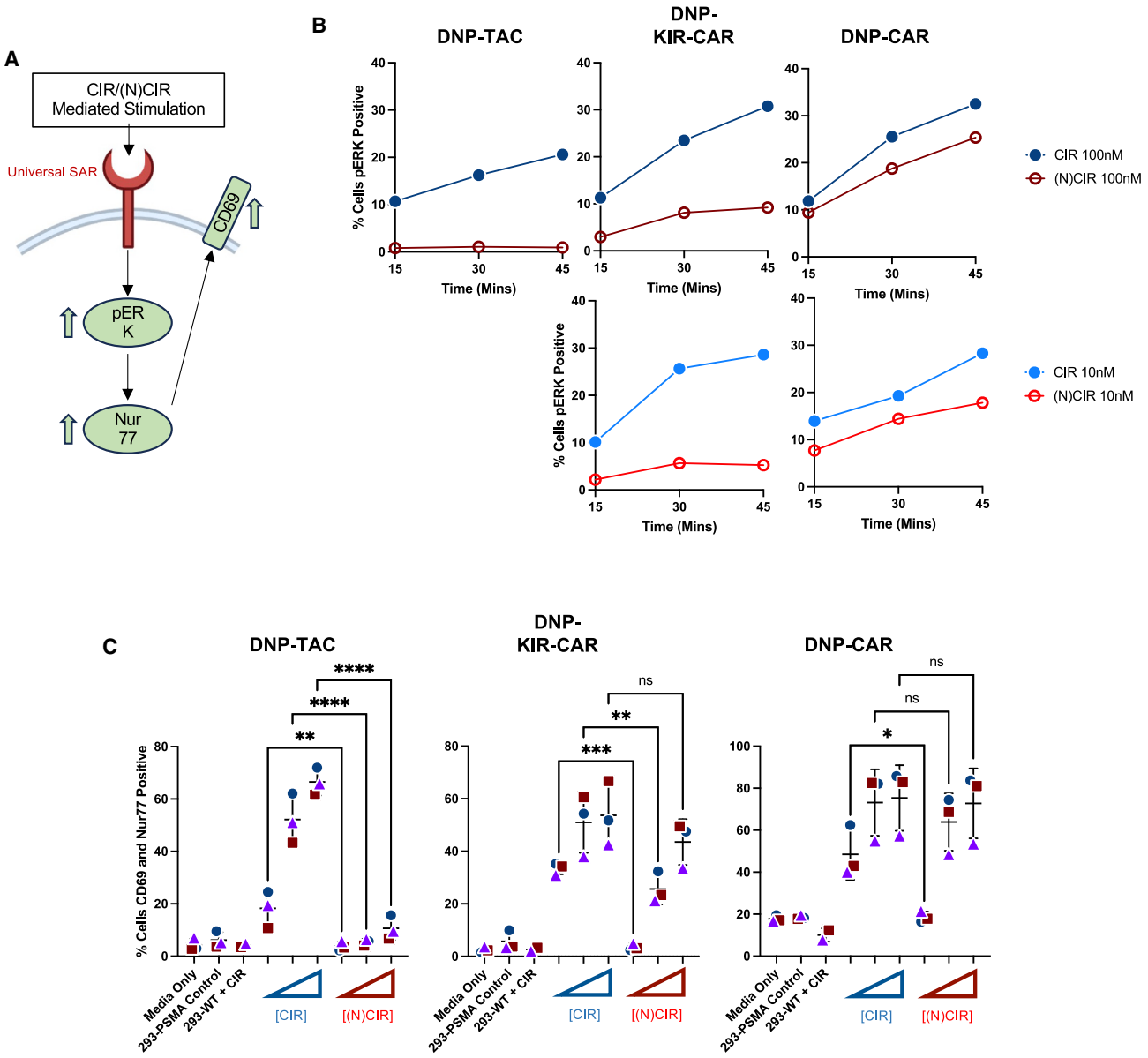

Figure 6. CIR-mediated anti-DNP SAR T-cell activation and tonic signaling

(A) Brief overview of signaling cascade in T cells. (B) Anti-DNP SAR-engineered αβ T cells were co-incubated with 293-PSMA cells in the presence 100 nM (dark colors; upper panels) or 10 nM (light colors; lower panels) of PSMA-CIR (blue) or PSMA-(N)CIR (red). Cells were fixed, permeabilized, and stained for phosphorylated ERK. The percentage of pERK-positive cells was plotted over a 45-min time course (see Figure S11 for gating). (C) Anti-DNP SAR engineered αβ T cells were co-cultured with PSMA-CIR (1 nM, 10 nM, 100 nM), PSMA-(N)CIR (1 nM, 10 nM, 100 nM) and 293-PSMA cells; increasing CIR/(N)CIR concentration is shown as a blue or red triangle, respectively. As negative controls, T cells were incubated in medium alone (Media Only), PSMA-expressing 293 in the absence of CIR (293-PSMA Control) or wild-type 293 and 100 nM PSMA-CIR (CIR +293-WT). CD69 and Nur77 were measured by flow cytometry. The y axis reflects the fraction of cells expressing both CD69 and Nur77. Three independent donors were tested—each donor is shown as an individual symbol (triangle, square, circle). Both CD4 and CD8 T cell population revealed the same results. Data for CD8+ T cells is shown here (see Figure S8 for gating). Statistical analysis for (C) was performed using two-way ANOVA with correction for multiple comparison (Tukey test) (*$p \leq 0.05$, **$p \leq 0.01$, ***$p \leq 0.001$, ****$p \leq 0.0001$, ns = not significant).

with 293-PSMA cells in the presence of varying doses of CIR and (N)CIR (Figure 6C). These data confirm differences in T cell activation in the presence of CIR vs. (N)CIR. In the case of DNP-TAC T cells, only the CIR could enable T cell activation at any concentration of adapter. DNP-KIR-CAR T cells displayed similar levels of activation in the presence of 100 nM CIR and (N)CIR, whereas the CIR was much more effective at producing T cell activation at limiting concentrations (most notably at 1 nM where the (N)CIR

had no activity). The DNP-CAR-T cells were the least affected by covalent attachment and differences between CIR and (N)CIR were only observed at the lowest concentration (1 nM). These data demonstrate that covalent engagement of SARs by the molecular adapter enhances activation of all SARs compared with non-covalent engagement. Collectively, the data in Figures 5 and 6 suggest that CIR functional enhancements are not due to an increased frequency of cell-cell conjugates or synapse formation, but rather a more robust activation signal being delivered through the SAR by covalent engagement.

DISCUSSION

We have described a novel non-enzymatic method to covalently attach molecular adapters using affinity-induced labeling chemistries that should have broad utlity across numerous bifunctional molecular adapter designs, including small molecules, proteins, and non-protein ligands. We have also extended the universal SAR platform to a variety of SAR scaffolds (TAC, CAR, and KIR-CAR). Our results clearly establish the value of covalent anchoring of the molecular adapter to the SAR. We have employed reactive electrophiles with differing reactive rates, rates of hydrolysis, and target amino acid specificity. While lysine reactive acylimidazole esters react faster, the more hydrolytically stable SuFEX group enables additional labeling of tyrosine and tryptophan residues; both chemistries display highly selective labeling of our universal SARs. Additionally, our results support the general utility and modularity of CIR design to target diverse tumor antigens and to enhance T cell tumoricidal function.

To date, the design of universal SARs has been limited to second-generation CARs, and for the most part, generated ternary complex with tumor cells using molecular adapters that employed non-covalent binding to elicit a response. Recent reports have described the use of large molecular weight bifunctional adapters (antibodies, DARPins) that form covalent bonds with the CAR through enzymatic linkage[14,16,31] and argued that the covalent linkage provides a functional advantage, although they have not provided robust mechanistic data to explain the value of covalent ligation of the molecular adapter. Our work extends the existing knowledge through intensive characterization of the influence of covalent ligation via molecular adapters using multiple covalent chemistries, multiple targeting ligands, and a variety of SARs.

We observed no difference in the frequency of conjugates being formed between T cells and tumor targets when programmed via CIRs or (N)CIRs, consistent with comparable ternary complex formation. However, we noted differences in the propagated signal intensity mediated by the two adapters revealing a novel role for covalency in the context of bifunctional molecular adapters beyond occupancy-driven effects. Mechanistically, the TAC, KIR-CAR, and CD28 CAR may initiate T cell signaling through different pathways, but all rely on adequate interaction time and ligation-dependent mechanical force to initiate activation of the T cell. We hypothesize the covalent bond formed between the SARs and the CIRs increases T cell activation through improved mechanics. On-going studies are assessing receptor movement, recycling, and clearance to further understand the adapter-receptor interaction.

With regard to the SARs themselves, these findings provide new insight into differential activation requirements, which reveal unexpected aspects of their biology. CARs display varying levels of basal signaling in the absence of antigen; a feature known as "tonic signaling," which has been well described in the literature,[41,42] while it has been reported that TAC and KIR-CAR have little tonic signaling.[32,33] In our experience, CAR-mediated tonic signaling raises the basal activation state, making the CAR-engineered cells easier to trigger relative to TAC-engineered cells (Moogk et al., unpublished data). A direct comparison of basal CD69 and Nur77 expression and spontaneous cytokine production betweeen SARs was used to define the following hierarchy for tonic signaling: CD28-CAR > KIR-CAR $\geq$ TAC. Interestingly, this trend paralleled the relative sensitivity of these SARs to activation by (N)CIRs and is inversely related to the magnitude of covalent functional enhancement via CIRs. These results cannot be explained on the basis of differences in receptor occupancy arguments alone, since both (N)CIR and CIRs engage a comparable fraction of SARs at the concentrations and timescales used in these assays. The DNP-CAR-T cells displayed the least benefit of covalent linkage to the molecular adapter in the context of the PSMA-directed molecular adapters, where the difference between the CIR and (N)CIR versions were significant but small. We believe this lower dependence on covalent linkage is a result of the higher tonic signaling observed with the CAR-T cells. It has been suggested that the tonic signal may be due to the presence of CARs at the cell surface in microclusters that are primed to activate,[42] as such, weaker interactions, such as those achieved with the (N)CIR may be sufficient to elicit anti-tumor effector functions and receptor signaling. This reduced threshold of signaling did not manifest in the context of a different tumor ligand (uPAR), where all SARs were critically reliant upon covalent attachment of the molecular adapter. Whether this difference was related to the tumor target itself, the uPAR ligand (a short peptide), or the chemistry used for that series of adapters remains to be determined. Regardless, the studies with the uPAR-directed CIR demonstrate that covalent attachment of the molecular adapter can greatly enhance the performance of a universal CAR-T cell, which is consistent with results using the SpyTag/SpyCatch system where enzymatic attachment of the molecular adapter enhanced cytotoxicity of CAR-T cells.[14]

DNP-TAC-T cells and DNP-KIR-CAR-T cells displayed an absolute benefit of covalent attachment in all experiments. Of these two platforms, the KIR-CAR platform is of greatest interest for further development. First, there is no measurable tonic signaling from the KIR-CAR similar to the TAC. Given that tonic signaling has been linked to premature exhaustion of engineered T cells and impaired therapeutic efficacy,[20] these two receptors would be preferable to a CAR. Second, while both TAC and KIR-CAR display no tonic signaling, T cell activation resulting from ligation of the KIR-CAR to a target cell via CIR leads to markedly enhanced effector functions over the TAC/CIR combination. This enhancement is most notable

in the context of proliferation, a key measure linked to improved therapeutic outcome. Whereas DNP-TAC T cells displayed very little proliferation at even the highest concentrations of CIR (100 nM), DNP-KIR-CAR T cells were activated to proliferate at the lowest concentration of CIR tested (1 nM); at this limiting concentration, the KIR-CAR outperformed all other SARs. For these reasons, our future work will focus on the KIR-CAR platform and we will optimize the SAR and CIR in parallel through iterative experimentation. The ultimate test of the SAR/CIR combination will come from *in vivo* models. We are presently developing ligands that are suitable for syngeneic and xenograft tumor models to enable a better understanding of T cell and CIR pharmacokinetics as it relates to therapeutic effect.

In conclusion, we have described a new class of small molecules that allow for affinity-induced labeling and functionalization of SARs toward tumor targets. We have shown that CIRs can be used in conjunction with a variety of SAR-T cells, including TAC, KIR-CAR, and CD28 CAR-T cells, as well our mechanistic interrogation of the molecular origins underlying covalent functional enhancements in receptor signaling reveal a unique benefit for covalency in drug development. These findings will guide the optimization of next-generation chemical immunotherapeutic technologies.

MATERIALS AND METHODS

Cell lines

LnCap cells (human prostate cancer cell line, obtained from ATCC) were cultured in RPMI 1640 (Gibco), supplemented with 10% FBS (Gibco), 2 mM L-glutamine (BioShop), 100 U/mL penicillin (Gibco), and 100 μg/mL streptomycin (Gibco). To generate nuclear red protein-expressing cell lines, parental LnCap cell lines were transduced with Nuclight Red lentivirus (Sartorious) encoding mKate2 and puromycin N-acetyltransferase at an MOI 3 and selected in culture media supplemented with 2.5 μg/mL puromycin (InvivoGen).

K562 and PC3 cell lines were cultured in RPMI 1640 (Gibco), supplemented with 10% FBS (Gibco), 2 mM L-glutamine (BioShop), 100 U/mL penicillin (Gibco), and 100 μg/mL streptomycin (Gibco), 10 mM HEPES (Roche Diagnostics), 1 mM sodium pyruvate (Sigma-Aldrich), 1 mM non-essential amino acids (Gibco), and 55 μM β-mercaptoethanol (Gibco). To generate cells for microscopy, parental K562 cell lines were transduced with lentivirus encoding PSMA fused to mCherry. These cells were flow sorted according to tNGFR transduction (co-transduction marker) using the BD FACSAria III.

HEK293T-WT, HEK293T-PSMA, PG13, and A172 eGFP cells were cultured in DMEM (Gibco), supplemented with 10% FBS (Gibco), 2 mM L-glutamine (BioShop), 10 mM HEPES (Roche Diagnostics), 100 U/mL penicillin (Gibco), and 100 μg/mL streptomycin (Gibco). HEK293 cells used for virus production were alternatively supplemented with 0.1 mg/mL normocin (InvivoGen). All cells were cultured at 37°C, 95% ambient air, 5% CO_2.

Receptor generation and gammaretrovirus production

The SPE7 variable heavy-variable light scFv was first designed using the crystal structure (PDB: 1OAU) and synthesized by Genescript. The human CD8α signal peptide was used for the TAC, DAP12 SAR, and CD28 CAR constructs. The anti-DNP scFv containing engineered receptors was cloned into the pRV100G vector. Gammaretrovirus was generated to be used for subsequent engineering of T cells. Briefly, PLAT-E cells were first transduced with the anti-DNP SAR containing plasmids (15 μg) and pCl Eco (15 μg) using using Opti-MEM (Gibco) and Lipofectamine 2000 (Thermo Fisher Scientific). Ecotropic gamma retrovirus was concentrated by centrifugation using Amicon Ultra-15 100 kDA centrifugal filter tubes (Millipore Sigma) and stored at −80°C. This ecotropic gammaretrovirus was then used to transduce PG-13 cells. PG-13 cells received 3 days of consecutive transduction. The PG-13s were scaled up and subsequently the virus containing supernatant produced by these cells was then filtered through a 0.45-μm filter (Thermo Scientific) and stored at −80°C to be used for T cell engineering.

Engineering of human T cells

Peripheral blood mononuclear cells (PBMCs) were obtained from healthy donors. In some cases, PBMCs were collected from commercial leukapheresis products (HemaCare and StemCell Technologies). PBMCs were isolated by Ficoll-Paque-Plus gradient centrifugation (GE Healthcare) and cryopreserved in inactivated human AB serum (Corning), containing 10% DMSO (Sigma-Aldrich), or Cryostor CS10 (Stemcell).

To produce primary human αβ T cells, 1×10^6 PBMCs were seeded in a 24-well plate and stimulated with ImunnoCult CD3/CD28/CD2 soluble activator (Stemcell) at a concentration of 25 μL/mL and cultured in RPMI 1640 (Gibco) containing 10% FBS (Gibco), 2 mM L-glutamine (BioShop), 10 mM HEPES (Roche Diagnostics), 1 mM sodium pyruvate (Sigma-Aldrich), 1 mM non-essential amino acids (Gibco), 55 μM β-mercaptoethanol (Gibco), 100 U/mL penicillin (Gibco), 100 μg/mL streptomycin (Gibco), 100 IU/mL recombinant human interleukin (rhIL)-2, and 10 ng/mL rhIL-7 (PeproTech). Forty-eight hours later, cells were transferred to a 24-well non-tissue culture-coated plate (Falcon) that was pre-coated with retronectin (10 μg/mL) and anti-DNP scFv SAR gamma retrovirus for transduction. Twenty-four hours later, 1 mL of T cell media supplemented with rhIL-2 (100 IU/mL,1.5 ng/mL) and rhIL-7 (10 ng/mL) (PeproTech) was added to each well. Forty-eight hours after media addition, the cells were washed with PBS and scaled into a larger vessel. Cells were cultured for a total period of 14 days prior to cryopreservation. T cells were cryopreserved in Cryostor CS10 (StemCell Technologies) according to the manufacturer's instructions.

Receptor expression determination via flow cytometry

Surface expression of SAR constructs was determined by staining with mouse anti-Myc (cat. no. 2276S, Cell Signaling Technology), followed by PE-conjugated goat anti-mouse immunoglobulin (Ig)G (cat. no. -115-116-146, Jackson ImmunoResearch). For αβ T cells, other phenotypic markers were detected with Pacific Blue-conjugated

mouse anti-human CD4 (cat. no. 558116, BD Pharmingen), AlexaFluor700-conjugated mouse anti-human CD8α (cat. no. 56-0086-82, Invitrogen), and VioBright FITC-conjugated mouse anti-human NGFR (cat. no. 130-113-423, Miltenyi Biotec). Flow cytometry data were collected with BD LSRII (BD Biosciences) or Cytoflex LX (Beckman Coulter) cytometer and analyzed using FlowJo vX (FlowJo) or FCS Express software (De Novo Software).

Receptor labeling analysis with CIR/(N)CIR

αβ T cells (1×10^6 cells) were labeled overnight at 4° in T cell media with 1 μM DNP-acyl imidazole-desthiobiotin (DTB CIR), DNP-Desthiobiotin (DTB (N)CIR), or just media. DNP-Glycine competitor was also added to some conditions at 200 μM as a competitor to assess labeling specificity. After the overnight incubation, the samples were washed three times with FACS buffer to remove any non-covalently bound molecule and stained with streptavidin-PE to assess labeling. The samples were also stained with Live/Dead Fixable Near-IR stain (cat. no. L10119, Invitrogen), Pacific Blue-conjugated mouse anti-human CD4 (cat. no. 558116, BD Pharmingen), and AlexaFluor700-conjugated mouse anti-human CD8α (cat. no. 56-0086-82, Invitrogen), allowing for appropriate gating on live αβ T cells. The samples were assessed for streptavidin-PE labeling via flow cytometry. Flow cytometry data were collected with BD LSRII (BD Biosciences) or Cytoflex LX (Beckman Coulter) cytometer and analyzed using FlowJo vX (FlowJo) or FCS Express software (De Novo Software).

For labeling time course studies, T cells were incubated with varying concentrations (10 nM, 100 nM, 1 μM) of either DTB CIR or DTB-(N)CIR for different time periods up to 3 h at room temperature in FACs buffer. The "0"-hour time point was the final time point and accounts for the 5-min period needed to spike in CIR/NCIR and spin down to stop labeling. After adding DNP-DTB CIR or DTB-(N) CIR to all time points, the cells were washed three times and stained for flow cytometry analysis as described above.

Nur77 and CD69 activation assessments

A total of 5×10^5 engineered anti-DNP SAR T cells and 5×10^5 Hek-293 PSMA or HEK293 WT tumor cells per sample were incubated for 0, 1, 2, 3, and 4 h at 37°C and 5% CO_2 with varying concentrations of PSMA-CIR, corresponding to PSMA-(N)CIR (1 nM, 10 nM, and 100 nM), or media alone. Cell surfaces were stained with Pacific Blue-conjugated mouse anti-human CD4 (cat. no. 558116, BD Pharmingen) and AlexaFluor700-conjugated mouse anti-human CD8α (cat. no. 56-0086-82, Invitrogen), VioBright FITC-conjugated mouse anti-human NGFR (cat. no. 130-113-423, Miltenyi Biotec), and anti-huCD69 (cat. no. 563835, BD Horizon), fixed, and permeabilized then fixed and permeabilized using the FoxP3 Transcription Factor Staining kit (cat. no. 00-5523-00, ThermoFisher), and stained intracellularly with PE-conjugated mouse anti-mouse Nur77 (cat. no. 12-5965-82, Invitrogen). Flow cytometry data were acquired and analyzed as indicated above. Three separate donor repeats were completed.

Cytokine production analysis

A total of 4×10^5 engineered T cells were stimulated with 4×10^5 HEK293T-PSMA, or HEK293T WT cells for 4 h at 37°C and 5% CO_2 in the presence of varying concentrations of PSMA-CIR or corresponding PSMA-(N)CIR (1 nM, 10 nM, 100 nM) and GolgiPlug (cat. no. 51-2301Kz, BD Biosciences). Cells were stained for surface expression of CD4 (BD Pharmingen) and CD8 (eBioscience), fixed, and permeabilized in Cytofix/Cytoperm buffer (cat. no. 51-2090KZ, BD Biosciences), and stained with APC-conjugated mouse anti-human IFN-γ (cat. no. 554702, BD Pharmingen), PE-conjugated rat anti-human IL-2 (cat. no. 554566, BD Pharmingen), and FITC-conjugated mouse anti-human TNF-α (cat. no. 554512, BD Pharmingen). Flow cytometry data were acquired and analyzed as indicated above. The assay was repeated with A172 and A172 uPAR CRISPR knockout (A172 uPAR KO) cell lines with uPAR-CIR and corresponding uPAR-(N)CIR.

In vitro cytotoxicity assay

LNCaP prostate cancer cells were engineered with Nuclight Red lentivirus (Sartorius, cat. no. 476). A172 glioblastoma cells were engineered with eGFP lentivirus made in house. In these experiments 5E3 tumor cells per well were pre-plated in a 96-well flatbottom plate overnight. The next day anti-DNP SAR αβ T cells were added to the tumor cells at an effector-to-target ratio of 8:1. Also added to the wells were the appropriate tumor-targeting CIRs or (N)CIRs at various concentrations (1 nM, 10 nM, 100 nM). The three components were co-cultured for 3–4 days at 37°C and 5% CO_2 in the Sartorius Incucyte S3 Live cell imaging system with nine images per well taken every 8 h. Three separate PBMC donor samples were analyzed with each donor sample run in triplicate. The number of LnCap cells per well at each time point was calculated using the Incucyte cell-by-cell analysis software and plotted to observe tumor growth. For the A172 eGFP cells, the green image mean for each image was used to determine tumor cell growth. The area under the growth curve (AUC) was analyzed using PRISM GraphPad and used as a metric for tumor cell growth for these data. The larger the area, the greater the tumor cell growth that occurred over the incubation period. The area under the curve for the tumor alone control control and each condition were used to calculate the % cytotoxicity.

Percent cytotoxicity was calculated as follows:

$$\%\ \text{Cytotoxicity} = \left(\frac{\text{AUC Tumor Alone} - \text{AUC Sample}}{\text{AUC Tumor Alone}}\right) \times 100\%$$

To assess cytotoxicity of pre-labeled anti-DNP SAR T cells, we used an assay following the experimental setup as described above. The difference being that instead of co-culturing tumor cells, T cells, and adapter together over the duration of the experiment, cells were pre-incubated for 1 h at 37° with either 1 μM PSMA-CIR, PSMA-(N)CIR, or media without adapter, and washed three times with T cell media prior to seeding with tumor cells. These were then seeded with LnCap Nuclight Red tumors cells in the same manner as

described above. Live cell imaging and data analysis was performed in the same manner as described above.

Proliferation assay

Anti-DNP SAR-engineered T cells (5E5 cells) labeled with CTV dye (cat. no. C34557, Invitrogen) were incubated with PSMA-CIR or PSMA-(N)CIR, and with HEK293TM-PSMA or HEK293-WT tumor targets at an effector:target ratio of 1:1, or left unstimulated in media. All proliferation assay samples were incubated for 3 days at 37°C and 5% CO_2. Cells were then stained with live/dead fixable near-IR stain (cat. no. L10119, Invitrogen), PerCP-Cy5.5-conjugated mouse anti-human CD8α (cat. no. 45-0088-42, eBioscience), Alexa Fluor 700-conjugated mouse anti-human CD4 (cat. no. 56-0048-82, eBioscience), VioBright FITC-conjugated mouse anti-human NGFR (cat. no. 130-113-423, Miltenyi Biotec), and BV605-conjugated mouse anti-human CD3 (cat. no. 300460 BioLegend). Flow cytometry data were acquired as indicated above. Results were analyzed with FCS Express (De Novo Software) by determining the starting generation peak based on the unstimulated sample and using the software proliferation package for fitting a proliferation model and collecting corresponding statistics, such as percent divided. FlowJo analysis software was used to generate histogram CTV dilution curves.

Microscopy studies

Microscopy studies were completed on the Nikon A1R Inverted confocal microscope. To study conjugation events, anti-DNP SAR T cells were pre-incubated with 200 nM PSMA-CIR, PSMA-(N)CIR, or media alone for 1 h at 37°C and 5% CO_2. These T cells were then co-incubated with K562 tumor cells engineered to express a PSMA-mCherry fusion protein. T cells and tumor cells were co-cultured at an E:T of 3:2 in 200 μL in a 1.5-mL Eppendorf tube with final concentration of 100-nM adapter. The cells were spun up to 16,000 × *g*, quickly stopping the spin to perform a quick pellet of the cells. These cell pellets were then incubated at 37°C for 10 min in a water bath. Following this incubation, the pellets were gently resuspended in serum-free media and plated into μ-Slide 8-well microscope slides (cat. no. 80826, Ibidi) for 20 min at 37°C and 5% CO_2. Each well was gently washed with 200 μL of PBS and then fixed with 200 μL of 2% PFA in PBS for 20 min at 4°C, subsequently stained with Alexa Fluor 647-conjugated mouse anti-human CD45 (cat. no. 304056, Biolegend), and stored in mounting medium containing DAPI (cat. no. 50011, Ibidi). To analyze the percentage of T cells conjugated to a tumor cell, tiled 8 × 8 images were collected using a ×20 objective and a Hamamatsu Orca Flash 4.0 V3 sCMOS with 82% High Quantum Efficiency camera. Images were analyzed using QuPath image analysis software.[43] Using the classification tool built into QuPath, T cell counts were generated using total cell count subtracted by tumor cell count. Each large image was manually analyzed for enumeration of cell conjugates. The number of conjugates was divided by the total T cell count to yield percentage of conjugated T cells.

To study both CD45 clearance and tyrosine phosphorylation at the immune synapse, samples were prepared in the same method as above but fixed with Cytofix (cat. no. 554655, BD Biosciences), stained with Alexa Fluor 647-conjugated mouse anti-human CD45 (cat. no. 304056, Biolegend), permeabilized with perm/wash buffer (cat. no. 554723, BD Biosciences), followed by staining with Alexa Fluor 488-conjugated mouse anti-phosphotyrosine (cat. no. 309306, Biolegend). Images were collected on the Nikon A1R Inverted confocal microscope with a ×60 oil immersion objective and laser scanning confocal acquisition - A1-DU4G HD with 4-channel PMT (2 GAASP high-sensitivity PMT; 2 PMT). Images of all conjugated cells were taken with 0.17-μm resolution. Single-plane images were taken where the cells were found to be in focus. The FIJI image analysis package[44] was used to analyze the images. Background subtraction was performed on all images prior to analysis. For quantification of CD45 clearance, the mean intensities of the Alexa Fluor 647 signal along a line drawn at the synapse and four other regions around the cell membrane were extracted using the line tool. The mean intensity of the four regions around the cell were averaged to yield the base intensity on the membrane of the cell. The percent of CD45 clearance was then calculated as $\%\text{CD45 Clearence} = 1 - \left(\frac{\text{MFI Synapse}}{\text{Average MFI Cell}}\right) \times 100\%$. For *p*-Tyr analysis, the rectangle tool was used to draw a box around the cell-to-cell contact region. The integrated intensity of the Alexa Fluor 488 within this region was extracted for each cell and compared between CIR and NCIR.

pERK phosphoflow

Anti-DNP engineered T cells were pre-incubated with 200 nM or 20 nM of PSMA-CIR, PSMA-(N)CIR, or media alone for 1 h at 37°C and 5% CO_2. A total of 5×10^5 engineered anti-DNP T cells were stimulated with 5×10^5 HEK293T-PSMA cells in a 24-well plate for 15, 30, and 45 min at 37°C and 5% CO_2 in the presence of either 100 nM or 10 nM final concentration of adapter. Cells were fixed at 37°C and 5% CO_2 with Cytofix (cat. no. 554655, BD Biosciences) for 10 min, followed by permeabilization on ice with pre-chilled perm buffer III (cat. no. 558050, BD Biosciences) for 30 min, and subsequent staining with Alexa Fluor 647 Mouse anti-ERK 1/2 (pT202,pY204) (cat. no. 612593, BD Biosciences). Data were collected on the Cytoflex LX (Beckman Coulter) cytometer and analyzed using FCS Express software (De Novo Software).

DATA AND CODE AVAILABILITY

The data presented in this study are available on request from the corresponding author.

SUPPLEMENTAL INFORMATION

Supplemental information can be found online at https://doi.org/10.1016/j.omton.2024.200842.

ACKNOWLEDGMENTS

This research was funded by support from the Samuel Family Foundation, CIHR, NSERC, CRS, and BioCanRx. N.J.S. received support from the Canada Graduate Scholarship CIHR (Funding Reference Number: 187472) and the Ontario Graduate Scholarship. A.E.M.,

B.O.M.L., and E.K. received support from the Canada Graduate Scholarship. J.L.B. was supported by the Canadian Research Chair in Translational Immunology and the John Bienenstock Chair in Molecular Medicine. Data and materials are available from the authors under a data or material transfer agreement.

AUTHOR CONTRIBUTIONS

Contribution: N.J.S., A.F.R., and J.L.B. designed the experiments. N.J.S. performed molecular and cellular work. N.J.S., A.F.R., and J.L.B. interpreted experimental results and wrote the manuscript. All authors read and approved the manuscript.

DECLARATION OF INTERESTS

J.L.B. has ownership interest in and receives research funding from Triumvira Immunologics Inc. N.J.S., A.F.R., A.E.M., and J.L.B. are co-inventors on a patent related to TAC receptors. J.L.B. is a co-inventor on several patents related to TAC receptors and oncolytic viruses. N.J.S., A.F.R., B.P.M.L., and J.L.B., are co-inventors on a patent related to CIRs. N.J.S., E.K., A.E.M., A.F.R., B.P.M.L., and J.L.B. are co-inventors on a patent related to universal SAR-directed CIRs.

REFERENCES

1. Singh, S., Tian, W., Severance, Z.C., Chaudhary, S.K., Anokhina, V., Mondal, B., Pergu, R., Singh, P., Dhawa, U., Singha, S., and Choudhary, A. (2023). Proximity-inducing modalities: the past, present, and future. Chem. Soc. Rev. *52*, 5485–5515. https://doi.org/10.1039/d2cs00943a.

2. Gerry, C.J., and Schreiber, S.L. (2020). Unifying principles of bifunctional, proximity-inducing small molecules. Nat. Chem. Biol. *16*, 369–378. https://doi.org/10.1038/s41589-020-0469-1.

3. Stevanovic, S., Draper, L.M., Langhan, M.M., Campbell, T.E., Kwong, M.L., Wunderlich, J.R., Dudley, M.E., Yang, J.C., Sherry, R.M., Kammula, U.S., et al. (2015). Complete regression of metastatic cervical cancer after treatment with human papillomavirus-targeted tumor-infiltrating T cells. J. Clin. Oncol. *33*, 1543–1550. https://doi.org/10.1200/JCO.2014.58.9093.

4. Sim, G.C., Chacon, J., Haymaker, C., Ritthipichai, K., Singh, M., Hwu, P., and Radvanyi, L. (2014). Tumor-infiltrating lymphocyte therapy for melanoma: rationale and issues for further clinical development. BioDrugs *28*, 421–437. https://doi.org/10.1007/s40259-014-0097-y.

5. Maude, S.L., Frey, N., Shaw, P.A., Aplenc, R., Barrett, D.M., Bunin, N.J., Chew, A., Gonzalez, V.E., Zheng, Z., Lacey, S.F., et al. (2014). Chimeric antigen receptor T cells for sustained remissions in leukemia. N. Engl. J. Med. *371*, 1507–1517. https://doi.org/10.1056/NEJMoa1407222.

6. Heslop, H.E., Slobod, K.S., Pule, M.A., Hale, G.A., Rousseau, A., Smith, C.A., Bollard, C.M., Liu, H., Wu, M.F., Rochester, R.J., et al. (2010). Long-term outcome of EBV-specific T-cell infusions to prevent or treat EBV-related lymphoproliferative disease in transplant recipients. Blood *115*, 925–935. https://doi.org/10.1182/blood-2009-08-239186.

7. D'Angelo, S.P., Melchiori, L., Merchant, M.S., Bernstein, D., Glod, J., Kaplan, R., Grupp, S., Tap, W.D., Chagin, K., Binder, G.K., et al. (2018). Antitumor Activity Associated with Prolonged Persistence of Adoptively Transferred NY-ESO-1 (c259)T Cells in Synovial Sarcoma. Cancer Discov. *8*, 944–957. https://doi.org/10.1158/2159-8290.CD-17-1417.

8. June, C.H., and Sadelain, M. (2018). Chimeric Antigen Receptor Therapy. N. Engl. J. Med. *379*, 64–73. https://doi.org/10.1056/NEJMra1706169.

9. Majzner, R.G., and Mackall, C.L. (2018). Tumor Antigen Escape from CAR T-cell Therapy. Cancer Discov. *8*, 1219–1226. https://doi.org/10.1158/2159-8290.CD-18-0442.

10. Chung, H., Jung, H., and Noh, J.Y. (2021). Emerging Approaches for Solid Tumor Treatment Using CAR-T Cell Therapy. Int. J. Mol. Sci. *22*, 12126. https://doi.org/10.3390/ijms222212126.

11. Safarzadeh Kozani, P., Safarzadeh Kozani, P., and Rahbarizadeh, F. (2021). Novel antigens of CAR T cell therapy: New roads; old destination. Transl. Oncol. *14*, 101079. https://doi.org/10.1016/j.tranon.2021.101079.

12. Minutolo, N.G., Hollander, E.E., and Powell, D.J., Jr. (2019). The Emergence of Universal Immune Receptor T Cell Therapy for Cancer. Front. Oncol. *9*, 176. https://doi.org/10.3389/fonc.2019.00176.

13. Sutherland, A.R., Owens, M.N., and Geyer, C.R. (2020). Modular Chimeric Antigen Receptor Systems for Universal CAR T Cell Retargeting. Int. J. Mol. Sci. *21*, 7222. https://doi.org/10.3390/ijms21197222.

14. Minutolo, N.G., Sharma, P., Poussin, M., Shaw, L.C., Brown, D.P., Hollander, E.E., Smole, A., Rodriguez-Garcia, A., Hui, J.Z., Zappala, F., et al. (2020). Quantitative Control of Gene-Engineered T-Cell Activity through the Covalent Attachment of Targeting Ligands to a Universal Immune Receptor. J. Am. Chem. Soc. *142*, 6554–6568. https://doi.org/10.1021/jacs.9b11622.

15. Kvorjak, M., Ruffo, E., Tivon, Y., So, V., Parikh, A.B., Deiters, A., and Lohmueller, J. (2023). Conditional control of universal CAR T cells by cleavable OFF-switch adaptors. Preprint at bioRxiv *142*, 6554. https://doi.org/10.1101/2023.05.22.541664.

16. Ruffo, E., Butchy, A.A., Tivon, Y., So, V., Kvorjak, M., Parikh, A., Adams, E.L., Miskov-Zivanov, N., Finn, O.J., Deiters, A., and Lohmueller, J. (2023). Post-translational covalent assembly of CAR and synNotch receptors for programmable antigen targeting. Nat. Commun. *14*, 2463. https://doi.org/10.1038/s41467-023-37863-5.

17. Lee, Y.G., Marks, I., Srinivasarao, M., Kanduluru, A.K., Mahalingam, S.M., Liu, X., Chu, H., and Low, P.S. (2019). Use of a Single CAR T Cell and Several Bispecific Adapters Facilitates Eradication of Multiple Antigenically Different Solid Tumors. Cancer Res. *79*, 387–396. https://doi.org/10.1158/0008-5472.CAN-18-1834.

18. Rong, L., Lim, R.M., Yin, X., Tan, L., Yang, J.H., and Xie, J. (2022). Site-Specific Dinitrophenylation of Single-Chain Antibody Fragments for Redirecting a Universal CAR-T Cell against Cancer Antigens. J. Mol. Biol. *434*, 167513. https://doi.org/10.1016/j.jmb.2022.167513.

19. Kim, M.S., Ma, J.S.Y., Yun, H., Cao, Y., Kim, J.Y., Chi, V., Wang, D., Woods, A., Sherwood, L., Caballero, D., et al. (2015). Redirection of genetically engineered CAR-T cells using bifunctional small molecules. J. Am. Chem. Soc. *137*, 2832–2835. https://doi.org/10.1021/jacs.5b00106.

20. Cao, Y., Rodgers, D.T., Du, J., Ahmad, I., Hampton, E.N., Ma, J.S.Y., Mazagova, M., Choi, S.H., Yun, H.Y., Xiao, H., et al. (2016). Design of Switchable Chimeric Antigen Receptor T Cells Targeting Breast Cancer. Angew. Chem. Int. Ed. Engl. *55*, 7520–7524. https://doi.org/10.1002/anie.201601902.

21. Urbanska, K., Lanitis, E., Poussin, M., Lynn, R.C., Gavin, B.P., Kelderman, S., Yu, J., Scholler, N., and Powell, D.J., Jr. (2012). A universal strategy for adoptive immunotherapy of cancer through use of a novel T-cell antigen receptor. Cancer Res. *72*, 1844–1852. https://doi.org/10.1158/0008-5472.CAN-11-3890.

22. Cho, J.H., Collins, J.J., and Wong, W.W. (2018). Universal Chimeric Antigen Receptors for Multiplexed and Logical Control of T Cell Responses. Cell *173*, 1426–1438.e11. https://doi.org/10.1016/j.cell.2018.03.038.

23. Lohmueller, J.J., Ham, J.D., Kvorjak, M., and Finn, O.J. (2017). mSA2 affinity-enhanced biotin-binding CAR T cells for universal tumor targeting. OncoImmunology *7*, e1368604. https://doi.org/10.1080/2162402X.2017.1368604.

24. Ma, J.S.Y., Kim, J.Y., Kazane, S.A., Choi, S.H., Yun, H.Y., Kim, M.S., Rodgers, D.T., Pugh, H.M., Singer, O., Sun, S.B., et al. (2016). Versatile strategy for controlling the specificity and activity of engineered T cells. Proc. Natl. Acad. Sci. USA *113*, E450–E458. https://doi.org/10.1073/pnas.1524193113.

25. Rodgers, D.T., Mazagova, M., Hampton, E.N., Cao, Y., Ramadoss, N.S., Hardy, I.R., Schulman, A., Du, J., Wang, F., Singer, O., et al. (2016). Switch-mediated activation and retargeting of CAR-T cells for B-cell malignancies. Proc. Natl. Acad. Sci. USA *113*, E459–E468. https://doi.org/10.1073/pnas.1524155113.

26. D'Aloia, M.M., Caratelli, S., Palumbo, C., Battella, S., Arriga, R., Lauro, D., Palmieri, G., Sconocchia, G., and Alimandi, M. (2016). T lymphocytes engineered to express a CD16-chimeric antigen receptor redirect T-cell immune responses against immunoglobulin G-opsonized target cells. Cytotherapy *18*, 278–290. https://doi.org/10.1016/j.jcyt.2015.10.014.

27. Raj, D., Yang, M.H., Rodgers, D., Hampton, E.N., Begum, J., Mustafa, A., Lorizio, D., Garces, I., Propper, D., Kench, J.G., et al. (2019). Switchable CAR-T cells mediate remission in metastatic pancreatic ductal adenocarcinoma. Gut *68*, 1052–1064. https://doi.org/10.1136/gutjnl-2018-316595.

28. Landgraf, K.E., Williams, S.R., Steiger, D., Gebhart, D., Lok, S., Martin, D.W., Roybal, K.T., and Kim, K.C. (2020). convertibleCARs: A chimeric antigen receptor system for flexible control of activity and antigen targeting. Commun. Biol. *3*, 296. https://doi.org/10.1038/s42003-020-1021-2.

29. Lee, Y.G., Chu, H., Lu, Y., Leamon, C.P., Srinivasarao, M., Putt, K.S., and Low, P.S. (2019). Regulation of CAR T cell-mediated cytokine release syndrome-like toxicity using low molecular weight adapters. Nat. Commun. *10*, 2681. https://doi.org/10.1038/s41467-019-10565-7.

30. Qi, J., Tsuji, K., Hymel, D., Burke, T.R., Jr., Hudecek, M., Rader, C., and Peng, H. (2020). Chemically Programmable and Switchable CAR-T Therapy. Angew. Chem. Int. Ed. Engl. *59*, 12178–12185. https://doi.org/10.1002/anie.202005432.

31. Stepanov, A.V., Xie, J., Zhu, Q., Shen, Z., Su, W., Kuai, L., Soll, R., Rader, C., Shaver, G., Douthit, L., et al. (2024). Control of the antitumour activity and specificity of CAR T cells via organic adapters covalently tethering the CAR to tumour cells. Nat. Biomed. Eng. *8*, 529–543. https://doi.org/10.1038/s41551-023-01102-5.

32. Helsen, C.W., Hammill, J.A., Lau, V.W.C., Mwawasi, K.A., Afsahi, A., Bezverbnaya, K., Newhook, L., Hayes, D.L., Aarts, C., Bojovic, B., et al. (2018). The chimeric TAC receptor co-opts the T cell receptor yielding robust anti-tumor activity without toxicity. Nat. Commun. *9*, 3049. https://doi.org/10.1038/s41467-018-05395-y.

33. Wang, E., Wang, L.C., Tsai, C.Y., Bhoj, V., Gershenson, Z., Moon, E., Newick, K., Sun, J., Lo, A., Baradet, T., et al. (2015). Generation of Potent T-cell Immunotherapy for Cancer Using DAP12-Based, Multichain, Chimeric Immunoreceptors. Cancer Immunol. Res. *3*, 815–826. https://doi.org/10.1158/2326-6066.CIR-15-0054.

34. Lake, B., Serniuck, N., Kapcan, E., Wang, A., and Rullo, A.F. (2020). Covalent Immune Recruiters: Tools to Gain Chemical Control Over Immune Recognition. ACS Chem. Biol. *15*, 1089–1095. https://doi.org/10.1021/acschembio.0c00112.

35. Ashouri, J.F., and Weiss, A. (2017). Endogenous Nur77 Is a Specific Indicator of Antigen Receptor Signaling in Human T and B Cells. J. Immunol. *198*, 657–668. https://doi.org/10.4049/jimmunol.1601301.

36. Ploug, M., Østergaard, S., Gårdsvoll, H., Kovalski, K., Holst-Hansen, C., Holm, A., Ossowski, L., and Danø, K. (2001). Peptide-derived antagonists of the urokinase receptor. affinity maturation by combinatorial chemistry, identification of functional epitopes, and inhibitory effect on cancer cell intravasation. Biochemistry *40*, 12157–12168. https://doi.org/10.1021/bi010662g.

37. Llinas, P., Le Du, M.H., Gårdsvoll, H., Danø, K., Ploug, M., Gilquin, B., Stura, E.A., and Ménez, A. (2005). Crystal structure of the human urokinase plasminogen activator receptor bound to an antagonist peptide. EMBO J. *24*, 1655–1663. https://doi.org/10.1038/sj.emboj.7600635.

38. McCann, H.M., Lake, B.P.M., Hoffman, K.S., Davola, M.E., Mossman, K.L., and Rullo, A.F. (2022). Covalent Immune Proximity-Induction Strategy Using SuFEx-Engineered Bifunctional Viral Peptides. ACS Chem. Biol. *17*, 1269–1281. https://doi.org/10.1021/acschembio.2c00233.

39. Kapcan, E., and Rullo, A.F. (2023). A covalent opsonization approach to enhance synthetic immunity against viral escape variants. Cell Rep. Phys. Sci. *4*, 101258. https://doi.org/10.1016/j.xcrp.2023.101258.

40. Xiao, Q., Zhang, X., Tu, L., Cao, J., Hinrichs, C.S., and Su, X. (2022). Size-dependent activation of CAR-T cells. Sci. Immunol. *7*, eabl3995. https://doi.org/10.1126/sciimmunol.abl3995.

41. Chen, J., Qiu, S., Li, W., Wang, K., Zhang, Y., Yang, H., Liu, B., Li, G., Li, L., Chen, M., et al. (2023). Tuning charge density of chimeric antigen receptor optimizes tonic signaling and CAR-T cell fitness. Cell Res. *33*, 341–354. https://doi.org/10.1038/s41422-023-00789-0.

42. Long, A.H., Haso, W.M., Shern, J.F., Wanhainen, K.M., Murgai, M., Ingaramo, M., Smith, J.P., Walker, A.J., Kohler, M.E., Venkateshwara, V.R., et al. (2015). 4-1BB costimulation ameliorates T cell exhaustion induced by tonic signaling of chimeric antigen receptors. Nat. Med. *21*, 581–590. https://doi.org/10.1038/nm.3838.

43. Bankhead, P., Loughrey, M.B., Fernández, J.A., Dombrowski, Y., McArt, D.G., Dunne, P.D., McQuaid, S., Gray, R.T., Murray, L.J., Coleman, H.G., et al. (2017). QuPath: Open source software for digital pathology image analysis. Sci. Rep. *7*, 16878. https://doi.org/10.1038/s41598-017-17204-5.

44. Schindelin, J., Arganda-Carreras, I., Frise, E., Kaynig, V., Longair, M., Pietzsch, T., Preibisch, S., Rueden, C., Saalfeld, S., Schmid, B., et al. (2012). Fiji: an open-source platform for biological-image analysis. Nat. Methods *9*, 676–682. https://doi.org/10.1038/nmeth.2019.